4

A Double Line Frequency Ripple Control using Integral Sliding Mode for qZSI and eqSBI

In previous chapter, a SMC based controller was used to mitigate the SRCs in source by incorporating a low pass filter. The higher value of time constant resulted in a larger reduction in the SRCs, however, there is an upper limit to the time constant that can be used. In this chapter a ISMC based dual loop control is proposed. The dual loop consists of an outer voltage control loop and inner current control loop. The control law of both the controllers are added and is fed to the PWM generation logic as the shoot through duty cycle. The proposed control is verified for qZSI and eqSBI SSIs.

The conventional voltage source inverters (VSIs) are extensively used in industrial drive applications, electric traction, domestic equipment etc. The output ac voltage of a VSI depends on the modulation index with the maximum value of unity. Hence, the maximum output ac voltage cannot be more than the input dc voltage. In order to obtain higher ac voltage, either transformers are to be used or a separate dc-dc boost converter is to be used. This increases the cost and size of overall system. To achieve lower cost and compact size, single stage topologies such as Z-source inverter (ZSI) have been proposed in Fang Zheng Peng [2003b]. The ZSIs consists of 'X' shaped impedance network of inductor and capacitor. The ZSIs have drawbacks of discontinuous input currents and high stress on capacitors Anderson and Peng [2008]. To remove these drawbacks, the quasi-ZSI have been proposed. The qZSIs also consist of a network of two inductors and capacitors with lower ratings compared to ZSIs Shahparasti *et al.* [2010]. The voltage boosting is obtained by shorting the inverter legs without affecting the power stage of the inverter. This is called shoot through. In literature, different z-source networks (ZSN) have derived to obtain higher voltage gain and lower component stress. Topologies such as extended boost ZSI Gajanayake *et al.* [2009], switched inductor ZSI Nguyen *et al.* [2011] and trans-ZSI Qian *et al.* [2011] have been proposed. The class of ZSIs consists of two inductors and two capacitors which are required to be of same rating. For low power applications, using qZSI may not be suitable. Hence, various topologies of switched boost inverters (SBIs) are used depending on application. The SBIs consists of a single inductor and capacitor. However, compared to the ZSIs, it consists of an additional active switch which shares the shoot through signal along with the inverter legs. Different topologies of SBIs such as Inverse Watkins–Johnson topology Mishra *et al.* [2012]; Ravindranath *et al.* [2013], Current fed quasi-SBIs Nag and Mishra [2014], DC-link type SBIs Nguyen *et al.* [2015a] have been proposed in literature. The SSI topologies have found applications in dc nanogrids, electric vehicles, etc.
The input current of the SSIs consists of second order harmonic components along with dc and switching components. These low frequency oscillations have detrimental effects on the sources over a long run. These SRC affects the photo-voltaic (PV) panels by increasing its temperature. This reduces the power generation efficiency of the PV panels Kim *et al.* [2013]. The maximum power point tracking is also affected due to oscillations in current Liu *et al.* [2014]. The SRCs affect the battery terminals by depleting the electrodes. The SRCs must be limited to be within 8% of the load current IEE [2006, 2014]. The SRCs results in torque ripples in wind turbines. This may degrade the turbines over a long span of time Peña-Alzola *et al.* [2017]. Hence, the SRCs must be regulated to be within certain range. This can be done by- increasing the passive components or by adding an external circuit to absorb the ripple content. However, this may lead to increase of

size, weight and cost. The other way is to reduce SRC by implementing appropriate control. This method does not require any extra component and hence is cost effective.
Different control methodologies have been used with the aim of reducing source current ripple, increasing dc voltage gain factor and improve the dynamic response. A PID control with dual voltage and current control loops are used in Ellabban *et al.* [2012]. The bandwidth of the loops are to be chosen so as not to compromise with the dynamic performance. The non-linear control methodologies such as sliding mode control Rajaei *et al.* [2008] have been used to improve the dynamic performance. To reduce SRCs, methods such as bandpass filter inductor current feedback Zhang *et al.* [2014], notch filter inductor current feedback method Zhu *et al.* [2015] can be implemented. In qZSI, method proposed in Ge *et al.* [2016] can be used to reduce the SRC. Similarly, for eqSBI, a SRC component is added to the control law to cancel out the oscillations in the current. However, in all the above control methodologies, uncertainty in component value or external disturbance may degrade the performance of the SRC control used. The control must be able to mitigate SRC in presence of any uncertainty while keeping the dynamic response within acceptable limits.

In this chapter, an Integral Sliding Mode based Ripple Mitigation (ISMRM) methodology is proposed to reduce SRC in two single stage topologies i.e., qZSI and Embedded qSBIs. These two topologies have been chosen as EqSBI consists of an extra active switch compared to qZSI. This choice of topology will span various single stage inverter topologies. The ISMRM control is capable of SRC reduction and uncertainty mitigation in case of bounded disturbances in voltage and current measurements, and parametric uncertainties. The control law obtained from the ISMC is added to the control signal obtained from dual loop control. The resulting shoot through duty signal is then compared with the repeating sequences of desired frequency, and then signals are given to the inverter legs, and to the auxiliary switch in case of EqSBI. Addition of the ISMC loops makes the control robust against unknown bounded disturbances.
The chapter is organized as follows: Section 4.1 consists of the explanation of principle of ISMC. The section 4.2 consists of modeling and deriving the required transfer functions for qZSI and eqSBI. These transfer functions are used to design the dual loop control. The dual loop control designing is explained in Section 4.3. The proposed ISMRM for SRC reduction is explained in Section 4.4. The proposed control is verified through simulations, which is discussed in Section 4.5 and through experimentation, discussed in Section 4.6. The Section 4.7 concludes the chapter.

4.1 PRINCIPLE OF INTEGRAL SLIDING MODE CONTROL

The control methodologies such as PI, PID, feedback linearization etc. are used to control the SSIs, however, the dynamics degrade in presence of uncertainties. The uncertainties consist of modeling uncertainties, parametric variations, or some external disturbances. The concept of integral sliding mode (ISM) was proposed in Utkin and Jingxin Shi [1996]. In ISM, the sliding motion is enforced from the beginning of the system response Castanos and Fridman [2006]; Wen-Jun Cao and Jian-Xin Xu [2004]. The surface in the ISM consists of the comparison of the projection of the desired and the actual dynamics. The integral sliding mode control mitigates the uncertainties and restores the dynamics by generating appropriate control law. The ISMC is integrated with the nominal control which controls the plant within desired limits. Consider following system in state space form:

$$\dot{x} = f(x,t) + B(x)u \tag{4.1}$$

where, $x \in \mathbb{R}^n, u \in \mathbb{R}^m$, f(x,t) is the system matrix and B is the input matrix. In presence of some uncertainty, $\psi(x,t)$, the trajectories become:

$$\dot{x} = f(x,t) + B(x)u + \psi(x,t) \tag{4.2}$$

where, $\psi(x,t) \in \mathbb{R}^n$. The uncertainty $\psi(x,t)$ can be divided into two spaces. The uncertainty which is in the range space of the input matrix is known as the a matched uncertainty $\psi_m(x,t)$, and other uncertainties are called the unmatched uncertainty $\psi_u(x,t)$. Let v_m and v_u be two vectors such that,

$$Bv_m + B^{\perp}v_u = \psi_m(x,t) + \psi_u(x,t) = \psi(x,t) \tag{4.3}$$

where, $B^{\perp}$ is chosen such that its image is orthogonal to the system input matrix, i.e. $B^T B^{\perp}$=0. The objective is to design a control law u which consists of a nominal control law u_o and a non-linear ISM control law u_n, i.e. $u = u_o + u_n$ so as to mitigate the uncertainties. Substituting the control law and uncertainties in (4.4),

$$\dot{x} = f(x,t) + B(x)(u_o + u_n) + \psi_m(x,t) + \psi_u(x,t) \tag{4.4}$$

The non-linear control law u_n is to be designed so as to cancel out the matched uncertainties without any amplification of the unmatched uncertainties. To mitigate SRC in SSIs, the actual voltage and current is compared with the desired voltage and current which does not contain the SRCs.

4.2 MODELLING OF QZSI AND EQSBI

The single stage inverter topologies incorporate shoot through to boost the input dc voltage. During shoot though, the inverter legs are shorted in qZSIs. In eqSBIs, along with the inverter legs, the switch S_5 is also activated. The voltage and current distribution during shoot through and non shoot through stage for qZSI is shown in Fig.4.1a and Fig.4.1b respectively, and for eqSBI the shoot through and non shoot through stage is shown in Fig.4.1c and Fig.4.1d respectively. Impedance seen from inverter terminals towards the inductor near the source terminals is Z_L.

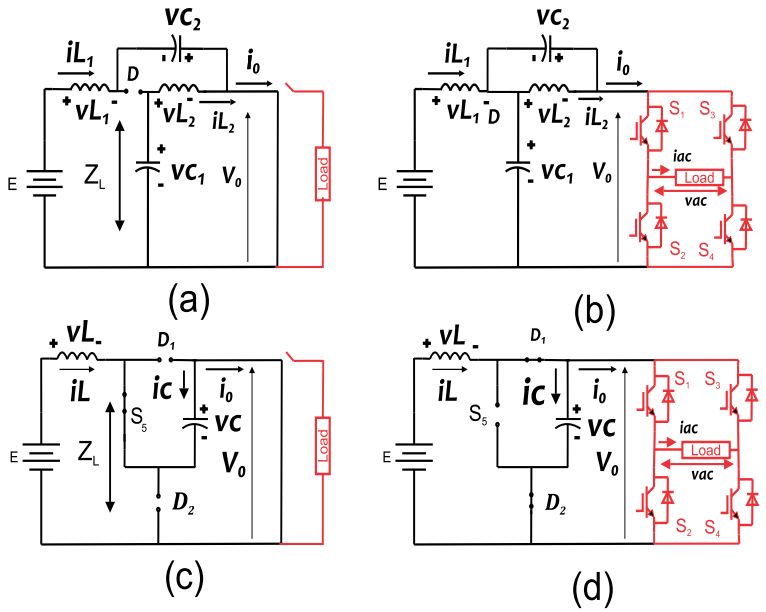

Figure 4.1 : Single stage inverter operation stages- (a) shoot through stage qZSI (b) non-shoot through stage qZSI (c) shoot through stage eqSBI (d) non-shoot through stage eqSBI

4.2.1 Modelling of Switched boost inverters (SBIs)

A SBI consists of inverter, an active switch S_5, an inductor L and a capacitor C. A SBI operates in two modes- shoot through and non-shoot through mode. This will be extended for qZSIs and eqSBIs.

In shoot through state,

$$L\frac{di_L}{dt} = v_c, \;\; v_{dc} = 0 \tag{4.5}$$

$$C\frac{dv_c}{dt} = -i_L, \;\; L_l\frac{di_o}{dt} = -i_o R_l \tag{4.6}$$

In non-shoot through state,

$$L\frac{di_L}{dt} = E - v_c, \;\; v_{dc} = v_c \tag{4.7}$$

$$C\frac{dv_c}{dt} = i_L - i_o, \;\; L_l\frac{di_o}{dt} = v_c - i_o R_l \tag{4.8}$$

where, L is inductor, C is capacitor, E is source voltage, v_c is capacitor voltage, i_L is inductor current, i_o is load voltage, L_l is load inductor, R_l is load resistance, v_{dc} is dc terminal voltage. Averaged model over a switching cycle can be written as,

$$L\frac{di_L}{dt} = E(1-d_{st}) + v_c(2d_{st}-1), \; v_{dc} = (1-d_{st})v_c \tag{4.9}$$

$$C\frac{dv_c}{dt} = (1-2d_{st})i_L + i_o(d_{st}-1), \; L_l\frac{di_o}{dt} = (1-d_{st})v_c - i_o R_l \tag{4.10}$$

Consider small perturbations in i_L, v_c and i_o, and shoot through duty cycle as - i_L=$I_L + \hat{i}_L$, v_c=$V_c + \hat{v}_c$, i_o=$I_o + \hat{i}_o$, d_{st}=$D_{st} + \hat{d}_{st}$. Using small signal perturbations, the $\frac{\hat{v}_c}{\hat{d}_{st}}$, $\frac{\hat{i}_L}{\hat{d}_{st}}$ and $\frac{\hat{v}_c}{\hat{i}_L}$ transfer functions is derived to be -

$$T_{pv} = \frac{\hat{v}_c}{\hat{d}_{st}} = \frac{b_2 s^2 + b_1 s + b_0}{a_3 s^3 + a_2 s^2 + a_1 s + a_0} \tag{4.11}$$

$$T_{pi} = \frac{\hat{i}_L}{\hat{d}_{st}} = \frac{c_2 s^2 + c_1 s + c_0}{d_3 s^3 + d_2 s^2 + d_1 s + d_0} \tag{4.12}$$

$$T_{pvi} = \frac{\hat{v}_c}{\hat{i}_L} = \frac{T_{pv}}{T_{pi}} \tag{4.13}$$

where,

$$a_0 = R_l(2D_{st}-1)^2, \; a_1 = L_l(2D_{st}-1)^2 + L(D_{st}-1)^2$$

$$a_2 = CLR_l, \; a_3 = CLL_l,$$

$$b_0 = -R_l(2D_{st}-1)(2Vc-E), \; b_2 = (I_o - 2I_L)LL_l$$

$$b_1 = -L_l(2D_{st}-1)(2Vc-E) + L(V_c(1-D_{st}) + R_l(I_o - 2I_L))$$

Above transfer functions are used to calculate the gains of dual loop control. The loop is designed such that the voltage loop has slower dynamics than the inner current loop. The overall objective to design the dual loop control is to improve the gain in low frequency range, and reduce gain in high frequency range. In state space form the state equations can be written as:

$$\dot{x} = Ax + Bu \tag{4.14}$$

where, $x = [\hat{i_L}, \hat{v_c}, \hat{i_o}]$, $u = \hat{d}$,

$$\begin{bmatrix} \dot{\hat{i}_L} \\ \dot{\hat{v}_c} \\ \dot{\hat{i}_l} \end{bmatrix} = \begin{bmatrix} 0 & (2D-1)/L & 0 \\ (1-2D)/C & 0 & (D-1)/C \\ 0 & (1-D)/L_l & -R_l/L_l \end{bmatrix} \begin{bmatrix} \hat{i_L} \\ \hat{v_c} \\ \hat{i_l} \end{bmatrix} \tag{4.15}$$

$$+ \begin{bmatrix} (2V_c - E)/L \\ (I_o - 2I_L)/C \\ -V_c/L_l \end{bmatrix} \hat{d}$$

Once the linear controllers G_v and G_i are designed, the ISMC is designed so as to mitigate any uncertainty such that the upper bound of uncertainty must be known.

4.2.2 Modelling of qZSI

The qZSI consists of two inductor and capacitors. To analyze a qZSI the inductors and capacitors are considered to be of same rating i.e. L_1=L_2=L, and capacitor C_1=C_2=C, as in Ge *et al.* [2016]; Ge *et al.* [2016b]. This makes the analysis simple. The averaged model of qZSI is derived to be-

$$L\frac{di_L}{dt} = (1-d)e + (2d-1)v_c - r_L i_L \tag{4.16}$$

$$C\frac{dv_c}{dt} = (1-2d)i_L - (1-d)i_o \tag{4.17}$$

where, e is the source voltage, d is the shoot through duty cycle, r_L is inductor resistance, i_o is ac load current, v_c is the voltage across the capacitor C. Consider small perturbations as $d = D + \hat{d}, i_L = I_L + \hat{i_L}, v_c = V_c + \hat{v_c}, e = E + \hat{e}, i_o = I_o + \hat{i_o}$, where, V_c, I_L, I_o, D are steady state operating values which are-

$$V_c = \frac{(1-D)E - r_L I_L}{(1-2D)}, \quad I_L = \frac{(1-D)I_o}{(1-2D)} \tag{4.18}$$

The small signal model around desired operating points are derived as:

$$\hat{\dot{x}} = A\hat{x} + B\hat{d} + C\hat{e} + D\hat{i_o} \tag{4.19}$$

where, $x = [\hat{i_L} \;\; \hat{v_c}]^T$

$$B = \begin{bmatrix} (2V_c - E)/L \\ (I_o - 2I_L)/C \end{bmatrix}, C = \begin{bmatrix} (1-D)/L \\ 0 \end{bmatrix},$$

$$A = \begin{bmatrix} -r_L/L & (2D-1)/L \\ (1-2D)/C & 0 \end{bmatrix}, D = \begin{bmatrix} 0 \\ (1-D)/C \end{bmatrix}$$

Using the above small signal model, the transfer functions- capacitor voltage to control G_{vd}, inductor current to control G_{id}, capacitor voltage to inductor current G_{vi} can be derived as:

$$G_{vd}\,|_{\hat{e}=0,\hat{i_o}=0} = \frac{(1-2D)(2V_c - E) + (r_L + sL)(I_o - 2I_L)}{s^2LC + sCr_L + (1-2D)^2} \tag{4.20}$$

$$G_{id}\,|_{\hat{e}=0,\hat{i_o}=0} = \frac{sC(2V_c - E) - (1-2D)(I_o - 2I_L)}{s^2LC + sCr_L + (1-2D)^2} \tag{4.21}$$

$$G_{vi}\,|_{\hat{e}=0,\hat{i_o}=0} = \frac{(1-2D)(2V_c - E) + (r_L + sL)(I_o - 2I_L)}{sC(2V_c - E) - (1-2D)(I_o - 2I_L)} \tag{4.22}$$

4.2.3 Modelling of eqSBI

Compared to qZSI, the eqSBI consists of an extra switch which is given the shoot through signal along with the inverter switches. The averaged model of eqSBI is derived to be Gambhir *et al.* [2019]:

$$L\frac{di_L}{dt} = e + (1-2d)v_c - i_L r_L \tag{4.23}$$

$$C\frac{dv_c}{dt} = (1-2d)i_L - (1-d)i_o \tag{4.24}$$

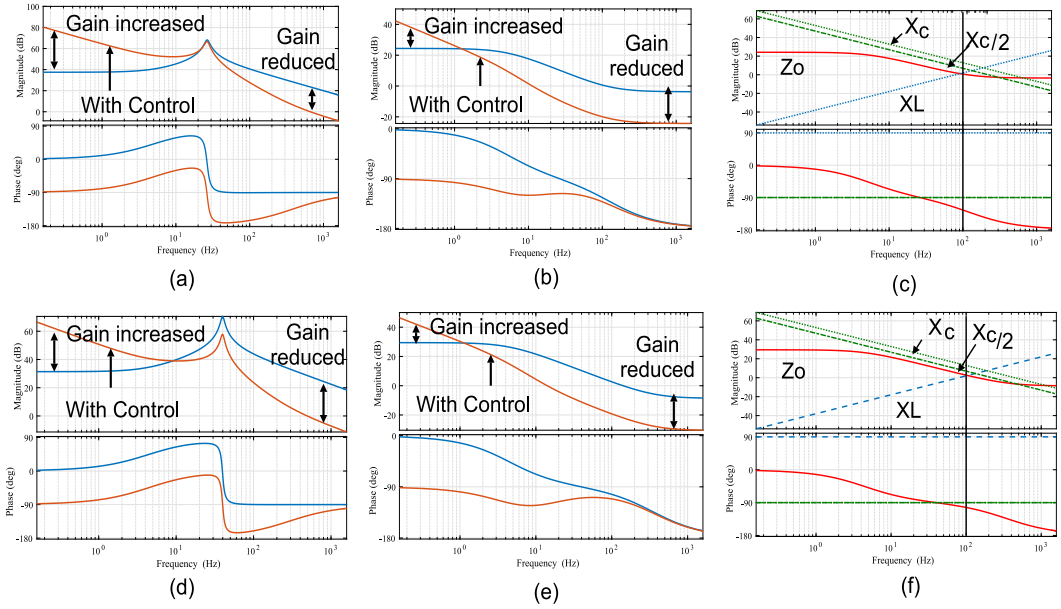

Figure 4.2 : Bode plots with and without dual loop control: (a) Current control loop qZSI, (b) Voltage control loop qZSI, (c) Impedance bode plot qZSI, (d) Current control loop eqSBI, (e) Voltage control loop eqSBI, (f) Impedance bode plot eqSBI

Similar to qZSI small signal modelling, small perturbations as $d = D + \hat{d}, i_L = I_L + \hat{i_L}, v_{c1} = V_c + \hat{v_c}, e = E + \hat{e}, i_o = I_o + \hat{i_o}$, where, V_c, I_L, I_o, D are steady state operating values which are,

$$V_c = \frac{E - r_L I_L}{(1-2D)}, \quad I_L = \frac{(1-D)I_o}{(1-2D)} \tag{4.25}$$

The A,B matrices of (4.19) for eqSBI are derived to be as follows:

$$A = \begin{bmatrix} -r_L/L & (2D-1)/L \\ (1-2D)/C & 0 \end{bmatrix}, B = \begin{bmatrix} 2V_c/L \\ (I_o - 2I_L)/C \end{bmatrix}$$

The matrix C is zero as small perturbation of input supply voltage is considered to be negligible. The D matrix remains same as for qZSIs The transfer functions G_{vd}, G_{id}, G_{vi} can be derived as:

$$G_{vd}\,|_{\hat{i_o}=0} = \frac{(1-2D)(2V_c) + (r_L + sL)(I_o - 2I_L)}{s^2LC + sCr_L + (1-2D)^2} \tag{4.26}$$

$$G_{id}\,|_{\hat{i_o}=0} = \frac{sC(2V_c) - (1-2D)(I_o - 2I_L)}{s^2LC + sCr_L + (1-2D)^2} \tag{4.27}$$

$$G_{vi}\,|_{\hat{i_o}=0} = \frac{2(1-2D)V_c + (r_L + sL)(I_o - 2I_L)}{2sCV_c - (1-2D)(I_o - 2I_L)} \tag{4.28}$$

These output to control transfer functions will be used to derive the controller gains in dual loop control.

4.3 DUAL LOOP CONTROL

The voltage across the capacitor and the inductor current is controlled using a dual loop control. The dual loop control consists of individual loops such that, the outer loop controls the voltage and generates the current reference for the inner inductor current control loop. The inner loop generates the shoot through duty cycle. The dual loop design process is shown in Figure 4.3. In case of qZSI, the transfer function T_{pi} is G_{id} in (4.21), T_{pv} is G_{vi} in (4.22). Similarly, for eqSBI, the transfer function T_{pi} is G_{id} in (4.27) and, T_{pv} is G_{vi} given in (4.28). The proportional and integral gains of inner and outer loop are designed such that Erickson and Maksimovic [2001]:

1. The low frequency gain of the system is increased and the high frequency gain is reduced.

2. To design the current controller G_i, the closed loop response is designed to have one-tenth the gain crossover frequency of the control to inductor current transfer function T_{pi}. The closed loop phase margin is chosen to be 60^o.

3. To design the outer loop, the current control loop gain is considered to be unity. Now, similar to inner loop designing, the outer closed loop gain crossover frequency is taken to be one-fifteenth of the open loop gain crossover frequency of inductor current to capacitor voltage transfer function T_{pv}. Further, the phases margin here, is similar to the inner loop case.

4. The bode plot of current loop response for qZSI is shown in Figure 4.2(a). It can be observed that the low frequency gain has been improved. The bode plot of outer loop is shown in Figure 4.2(b). Similarly, inner loop and outer loop bode plots for eqSBI are shown in Figure 4.2(d) and Figure 4.2(e) respectively.

4.3.1 Impedance analysis

The bode plot of the impedance seen from the inverter terminals of qZSI is shown in Figure 4.2(c). It can be observed that at $2f_{ac}$ (100Hz), the magnitude of Z_L is less than the X_c. As a result, the SRCs propagate to the source instead of being absorbed by the capacitor. The impedance Z_L is less even when the capacitance value is doubled i.e. $X_c = 1/s(2C)$. Similar plots are obtained for eqSBI in Figure 4.2(f). Hence, instead of increasing the capacitance, it would be fruitful to increase the impedance of inductor virtually, as bulkier capacitor leads to increase of size and weight of the converters. To reduce the cost electrolytic capacitors are used however, they are not reliable and have comparatively smaller lifetime Falck *et al.* [2018]. The crossover frequencies of the inner and outer control loops are more than $2f_{ac}$. Hence, the references generated by the outer voltage control loop and inner current control loop may contain second order components. This further affects the shoot through duty cycle. Reduction of these ripples by reducing the gain crossover frequencies degrades the dynamics of the converter. The estimation of second order ripple in the shoot through duty cycle d_{st} is analyzed in the next section.

4.3.2 Estimation of second order component in the d_{st}

The second order components in inductor current and capacitor voltage depends on the second order components in the d_{st} and output current. The inductor current to output current transfer function $G_{i_L i_o}$ and capacitor voltage to output current transfer G_{vcio} function for qZSI can be derived using (4.19) as in Gambhir *et al.* [2019]:

$$G_{i_L i_o} = \frac{(1-D)(1-2D)}{s^2LC + sCr_L + (1-2D)^2} \tag{4.29}$$

$$G_{v_c i_o} = \frac{(1-D)}{s^2LC + sCr_L + (1-2D)^2} \tag{4.30}$$

Any perturbation in inductor current i_L and terminal voltage v_c depends on perturbations in d_{st} and i_o as:

$$\hat{i}_L(s) = G_{id}(s)\hat{d}(s) + G_{iLio}\hat{i}_o(s) \tag{4.31}$$

$$\hat{v}_c(s) = G_{vd}(s)\hat{d}(s) + G_{vcio}\hat{i}_o(s) \tag{4.32}$$

The second order inductor current component must be zero. Hence, substitute $\hat{i}_L(t) = 0$ in (4.31), (4.32) and

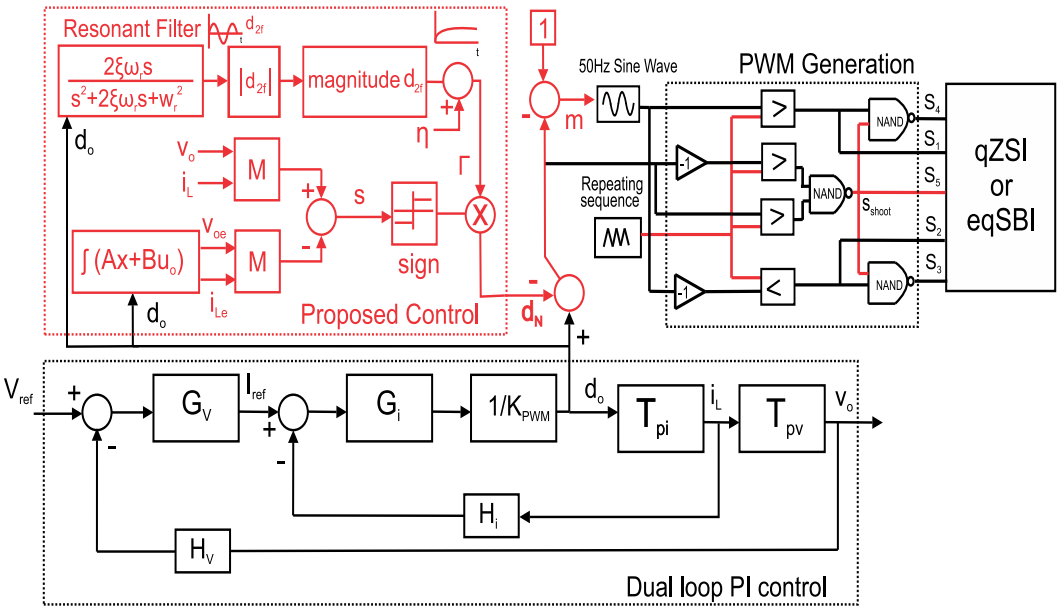

Figure 4.3 : Proposed ISMRM with dual loop control

solve for the second order component of shoot through duty cycle d_{2f} at $s = j2\omega$ as:

$$d_{2f} = \left(\frac{G_{iLio}(s)}{G_{vd}(s)G_{iLio}(s) - G_{vcio}(s)Gi_d(s)} \hat{v}_c(s) \right)_{s=j2\omega} \tag{4.33}$$

This second order component of d_{st} has to be mitigated using the proposed control.

4.4 PROPOSED ISM BASED DUAL LOOP CONTROL METHODOLOGY

In this section, the proposed ISM based dual loop methodology will be explained. Similar analysis can be done for either qZSIs or eqSBIs. When the matched and the unmatched uncertainties are taken into account, the dynamics become:

$$\dot{x}(t) = Ax(t) + Bd_{pi}(t) + \psi_m(t) + \psi_u(t,x) \tag{4.34}$$

The control law from the dual loop control d_{pi} consists of second order components: $d_{pi}(t) = d_o(t) + d_{2f}(t)$ where, d_o is the nominal control law value and d_{2f} is the second order oscillations. Let the non-linear control law d_n is to be added to the d_{pi} to mitigate the second order component. The overall control law becomes: $d = d_{pi} + d_n$. Substitute the uncertainties in terms of input matrix using (4.3), to obtain dynamics as,

$$\dot{x}(t) = Ax(t) + Bd_o(t) + Bd_{2f}(t) + Bd_n + Bv_m + B^{\perp}v_u \tag{4.35}$$

Now, choose a sliding surface as $s(t) = Mx(t) + y(t)$. The derivative of the surface with respect to time is, $\dot{s}(t) = M\dot{x}(t) + \dot{y}(t)$ where, $\dot{y}(t) = -M(Ax(t) + Bd_o)$ and initial condition $y(0) = -Mx(0)$. The matrix M is to be derived later in this section. Substitute the value of $\dot{x}$(t) from (4.35),

$$\dot{s}(t) = M(Ax(t) + Bd_o(t) + Bd_{2f}(t) + Bd_n + Bv_m + B^{\perp}v_u) + \dot{y}(t) \tag{4.36}$$

4.4.1 Without unmatched uncertainty ψ_u=0

When the unmatched uncertainty is negligible then the dynamics becomes:

$$\dot{s}(t) = M(Ax(t) + Bd_o(t) + Bd_{2f}(t) + Bd_n + Bv_m) + \dot{y}(t) \tag{4.37}$$

In this case the control law d_n must compensate for the second order component d_{2f} and matched uncertainty component Bv_m. Substituting values of $\dot{y}(t)$ in (6.28b),

$$\dot{s}(t) = MBd_{2f}(t) + MBd_n + MBv_m \tag{4.38}$$

Hence, when the dynamics reach the sliding manifold, $\dot{s} = 0$, and the equivalent control law d_{neq} can be derived by substituting $d_n = d_{neq}$ in (6.28c) as $d_{neq} = -d_{2f} - v_m$. Substituting this value of d_n the dynamics become,

$$\dot{x}(t) = Ax(t) + Bd_o(t) \tag{4.39}$$

Hence, the proposed control law cancels out the second order term in the PI generated control law which in turn results in mitigation of SRC.

4.4.2 With unmatched uncertainty ψ_u

When the unmatched uncertainty is finite then it must be ensured that the designed control law must not amplify these uncertainties. The control law is derived as:

$$\dot{s}(t) = MBd_{2f}(t) + MBd_n + M(Bv_m + B^{\perp}v_u) \tag{4.40}$$

Similar to the previous case, the equivalent control law is derived by substituting $\dot{s} = 0$, and solving for d_{neq} as $d_{neq} = -d_{2f} - B^{-1}(Bv_m + B^{\perp}v_u)$. The matrix B is not a square matrix, hence its pseudo inverse B^{+} can be substituted instead to of B^{-1}. Substitute the equivalent control value in (4.36), the dynamics become,

$$\dot{x}(t) = Ax(t) + Bd_o(t) + \underbrace{(I_n - B(MB)^{-1}M)}_{\gamma}B^{\perp}v_u \tag{4.41}$$

It must be observed from (6.28f), that the dynamics can get affected if the unmatched uncertainty γ is amplified. This leads to proper selection of the matrix M.

4.4.3 Selection of matrix M

The choice of the projection matrix M must be done such that it is the inverse of the input matrix B. However, the matrix B may not always be a square matrix. Hence, M must be Moore–Penrose (pseudo-inverse) of the matrix B, i.e. $M = (B^T B)^{-1}B^T$. As a result, the product MB results in an identity matrix I_n. Substituting this value and evaluating γ,

$$\gamma = (I_n - B(B^T B)^{-1}B^T) \tag{4.42}$$

It must be observed that on evaluating γ in (6.28f), the magnitude of $|\gamma B^{\perp}v_u| \leq |B^{\perp}v_u|$. Hence, the unmatched uncertainty is not amplified with such selection of matrix M.

4.4.4 Control law d_n and reachability condition

The control law derived from ISM depends on the values obtained from the comparison of the desired and actual dynamics. The desired dynamics consists of the inductor current with negligible SRC while the actual dynamics consists of the inductor current with high SRC component. This comparison in-turn generates the control law, which mitigates the second order component in the control signal of the PI controller. The control law d_n is chosen to be-

$$d_n = -\Gamma(MB)^{-1}\frac{s(t)}{||s(t)||} \tag{4.43}$$

To ensure the existence of the sliding motion, the η reachability condition, $s^T\dot{s} < -\eta||s||$ Edwards and Spurgeon [1998] must be satisfied. Substitute the value of d_n from (6.28h) to (6.28e), the differentiation of the sliding surface becomes,

$$\dot{s}(t) = MBd_{2f} - \Gamma\frac{s(t)}{||s(t)||} + M(Bv_m + B^{\perp}v_u) \tag{4.44}$$

Multiply by s^T and simplify,

$$s^T(t)\dot{s}(t) = s^T MBd_{2f} - \Gamma||s(t)|| + s^T MB^{\perp}v_u + MBv_m \tag{4.45}$$

$$s^T(t)\dot{s}(t) \leq ||s(t)||(||d_{2f}|| - \Gamma + ||MB^{\perp}v_u|| + ||MBv_m||) \tag{4.46}$$

Or to enforce the sliding motion, the parameter Γ can be evaluated to be,

$$\Gamma \geq (||d_{2f}|| + ||MB^{\perp}v_u|| + \eta + ||MBv_m||) \tag{4.47}$$

where, η is a positive constant. Hence, the value Γ should be greater than the sum of the second order component, matched and unmatched uncertainty and, some positive scalar constant.

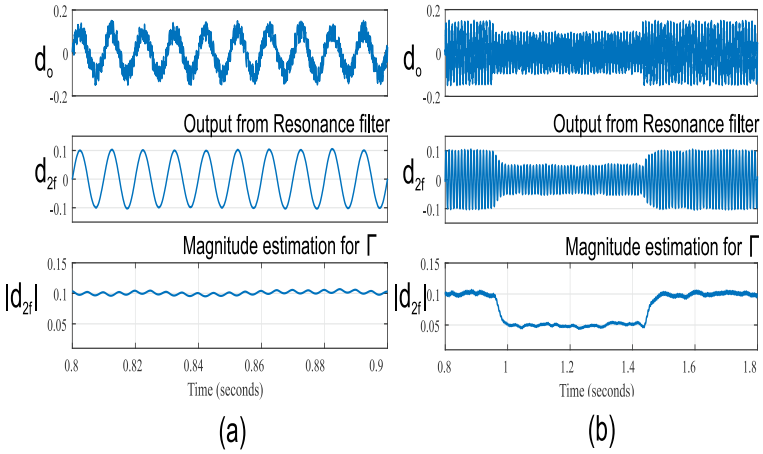

Figure 4.4 : Waveforms of d_o, and estimated magnitude of d_{2f}-(a) with constant d_o, (b) with varying d_o

4.4.5 Value and limitations of Γ

The control parameter Γ should be greater than the second order component defined in (4.33) for the proposed control to be effective. In actual conditions, the inverter ac load is varying in nature. Hence, the voltage and current second order oscillation amplitude is also varying. This increases the necessity of the proposed control to have SRC rejection capability with varying load conditions. To incorporate this, the value of Γ is obtained by passing the control signal of dual loop control through a resonant filter to obtain d_{2f} as shown in Fig.4.4. The amplitude of the second order component d_{2f} is hence extracted and fed as Γ in the ISM controller.

$$d_{2f} = \frac{2\zeta_r w_r s}{s^2 + 2\zeta_r w_r s + w_r^2} d_{pi} \tag{4.48}$$

In (4.48), $w_r = 2\pi f_{ac}$, $\zeta_r = 0.02$, and η is a positive constant as used in Cao *et al.* [2015]. The value of Γ should be greater than the d_{2f}. The magnitude to d_{2f} can be used to derive the inductor current and capacitor voltage oscillations (uncertainties) to be compensated as:

$$\Delta i_L = G_{id}|d_{2f}|,\ \Delta v_c = G_{vd}|d_{2f}| \tag{4.49}$$

The vectors v_m and v_u can be derived using (4.3) as:

$$[v_m \ \ v_u]^T = [B \ \ B^{\perp}]^{-1}[\Delta i_L \ \ \Delta v_c]^T \tag{4.50}$$

The values of d_{2f}, v_m, v_u can be derived and substituted in (4.47), to obtain the limits of Γ. Further, to ensure that the power stage of the qZSI or eqSBI is not shorted it must be ensured that the value of modulation index m must be less than the sum of d_n and d_{pi} i.e. $m < (1 - (d_n + d_{pi}))$.

4.5 SIMULATION RESULTS

The single stage inverter topologies- qZSI and eqSBI are simulated in Matlab 2018 to verify the proposed SRC control strategy. The dynamic performance with and without the proposed control , the increase of the virtual impedance, and the uncertainty mitigation of the proposed control strategy is verified under the following subsections.

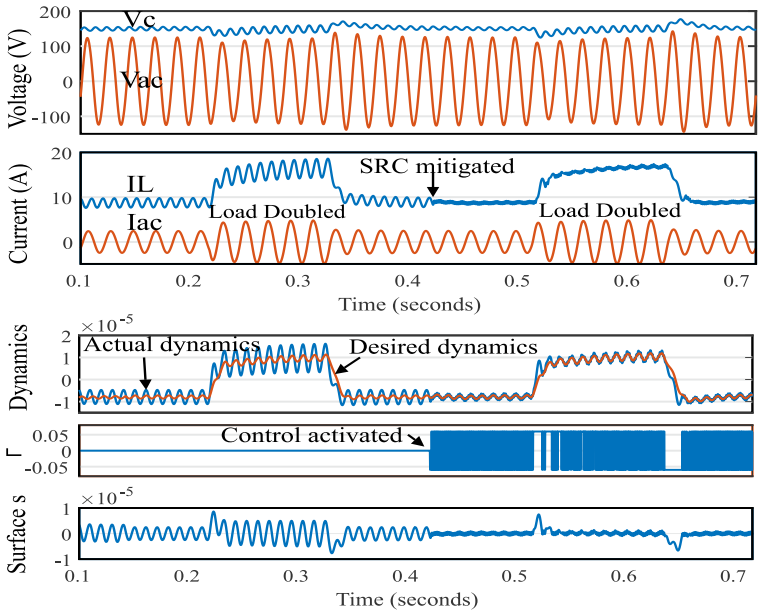

Figure 4.5 : Voltage and current waveforms and control parameters for qZSI

4.5.1 Dynamic performance

The voltage and current waveform for a qZSI is shown in Figure 4.6. Initially, with only dual loop, the source current has a high SRC component. The SRC component increases when the ac load is doubled. The proposed control is activated from time 0.41s onwards. The SRC reduces from 2A to 0.4A. It can be observed that the dynamic performance is not affected while the SRC is mitigated, when the load is doubled at 0.51s.

4.5.2 Uncertainty mitigation

The voltage reference of qZSI is perturbed with a known uncertainty of 5V about the reference. This results in large oscillations in input inductor current I_L of qZSI as shown in Figure 4.7(a). Once, the proposed control is implemented, the current I_L can be seen to have improved with lesser oscillations due to voltage reference uncertainty and SRC is also reduced, as shown in lower half of Figure 4.7(a). The SRC is mitigated considerably, and the voltage is within desired limits.

Similarly for the case of eqSBI, the voltage reference is again perturbed. This results in poor inductor current profile as shown in Figure 4.7(b). To mitigate the uncertainty and regulate the SRC, the proposed control is implemented and corresponding waveforms are shown in lower half of the Figure 4.7(b). It can be observed that the SRC is considerably reduced and current oscillations due to voltage reference perturbations are also mitigated. The reduction of SRC can be analyzed for qZSI through the THD magnitude shown in Figure 4.8. It can be observed that the THD at $2f_{ac}$ (i.e. 100Hz) is almost 11%. The THD magnitude after implementation of proposed control is shown in Figure 4.8(b). The THD at $2f_{ac}$ reduces to less than 1.2%. Furthur, overall THD which is 11.57% reduces to 3.93%. Hence, it can be concluded that the proposed control considerably reduces SRC and also mitigates any oscillations due to unknown bounded disturbances.

4.5.3 Virtual impedance analysis

The increase of impedance is observed through frequency sweep response of reference voltage of qZSI and eqSBI from 10Hz to 2000Hz. The increased impedance of qZSI can be observed from Figure 4.9(a) and of eqSBI can be seen from Figure 4.9(b). The impedance can be seen to have increased from 5dB to 20dB in case of qZSI and from 5dB to 23dB in case of eqSBI. Hence, the purpose of increasing impedance at $2f_{ac}$ is achieved.

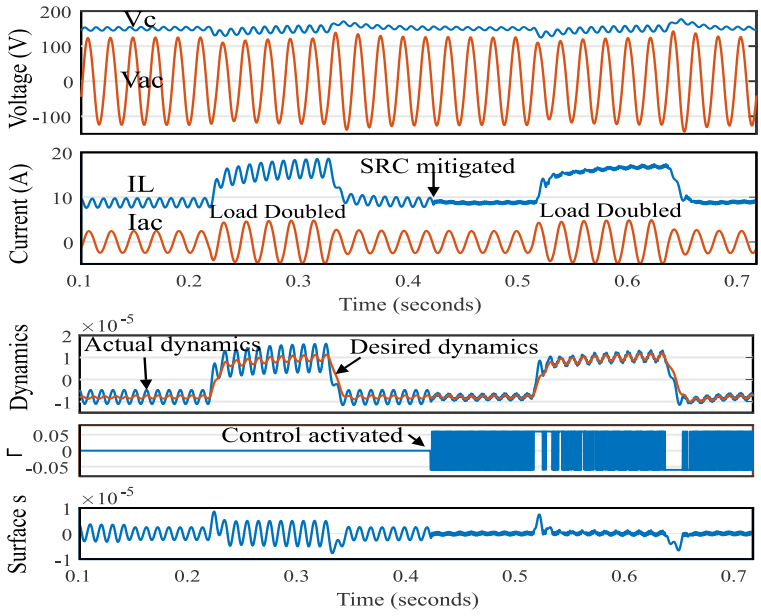

Figure 4.6 : Voltage and current waveforms and control parameters for qZSI

Table 4.1 : Simulation and experimental parameters

Parameters	qZSI	EqSBI
Inductor L,r_L (mH),(Ω)	0.8,0.1	0.8,0.1
Capacitor C (μF)	360	360
Carrier Frequency f_c (kHz)	10	10
Inverter Output frequency f_{ac} (Hz)	50	50
AC inverter loadr_{ac} (Ω)	100-50	100-50
Voltage reference,E (simulation) (V)	150,50	150,50
Voltage reference,E (hardware) (V)	90,30	90,30
Resonance Filter ω_r,ζ_r,m	2π100,0.02,0.6	
Magnitude ω_m,ζ_m	2π70,1	

4.6 EXPERIMENTAL RESULTS

Two different setups for qZSI and eqSBI are designed to verify the proposed control methodology experimentally, as shown in Figure 4.10. The control algorithm is implemented using the OPAL-RT Digital Simulator. The LEM HAL 50-S and Lem 25-P sensors are used to measure current and voltage respectively. The SKM75GB128D switches are used for inverter legs, FGH40N120ANTU IGBT is used as auxillary switch in eqSBI. A controlled 60V, 10A dc power supply is used to feed power to the converters. The inductor current, capacitor voltages, output load current and output ac voltages are analyzed with and without control for resistive and inductive loads for both qZSI and eqSBI.

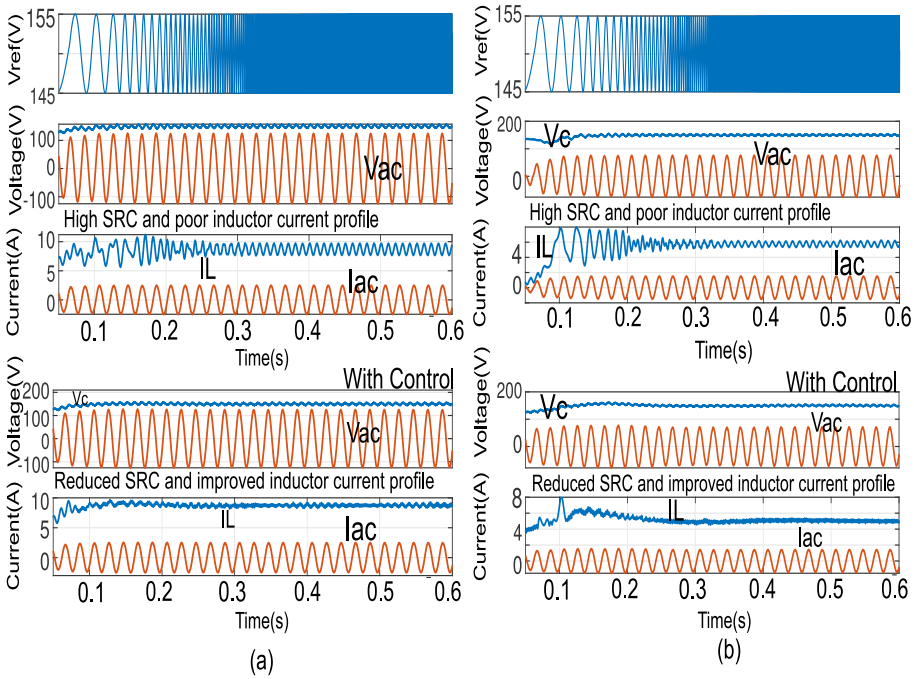

Figure 4.7 : Voltage and current waveforms with perturbed voltage reference for (a) qZSI and (b)eqSBI

4.6.1 SRC control for qZSIs

Resistive load

The voltage and current waveforms on dc and ac side are shown in Figure 4.11 and b. The capacitor voltage is controlled to be at 90V. A resistive load of 50Ω is applied at the output inverter terminals. As a result SRC of 1A propagate towards the source. When the proposed ISMRM is activated, the SRC content is mitigated. The capacitor voltage and ac voltage is controlled to be within desired limits. It can be observed that the SRC gets reduced to 0.2A from 1A. The waveforms with control activation and deactivation is shown in Figure 4.11.

Inductive and resistive load

The SRC mitigation must also be effective in case of inductive load. To verify this, the inverter fed load is made to be inductive in nature. An inductor of 5mH is put in series with resistive load of 100Ω. The SRC of 400mA can be seen at the dc source terminals as shown in Figure 4.13. To mitigate this SRC, the ISMRM control is activated and resultant waveforms are shown in Figure 4.14. It can be observed that the SRC reduces to 0.1A. Hence, proposed control effectively reduces the SRCs.

With Load variations

The SRC must be kept within limits even with load variations. To verify SRC reduction at load variations, the ac side load is varied such that it is reduced by 40% during T_2 and T_5, as shown in Figure 4.17.

Initially, the proposed control is not activated. The SRC varies from 1A to 0.5A with load variations. The proposed control is activated from $T_4 - T_6$. It can be observed that the SRC reduces to 0.2A, irrespective of load variations. The voltage drop during load increase is reduced by using the proposed control.

4.6.2 SRC control for eqSBI

In case of eqSBI, a load with inductance of 5mH and resistance of 100Ω is connected to the inverter terminals. This leads to SRC of 1A as shown in Figure 4.15. The output current lags the output ac voltage due to the inductive nature of load.

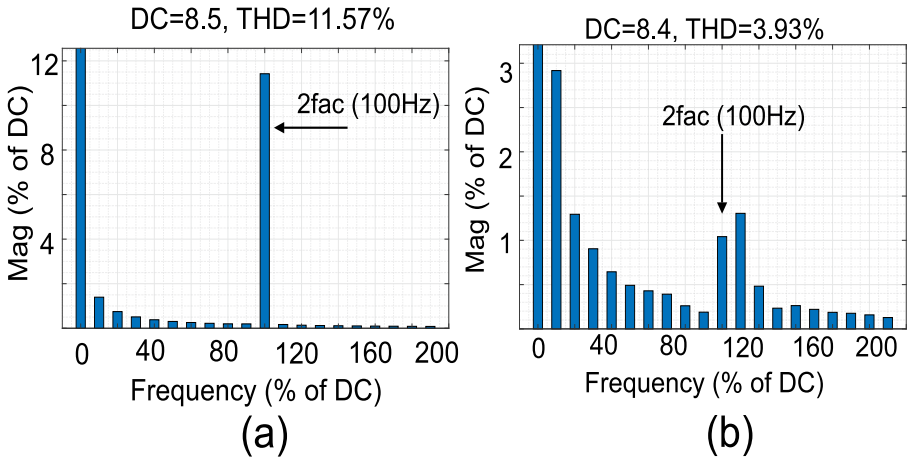

Figure 4.8 : FFT analysis: (a) THD plot of inductor current without control-11% of load current at $2f_{ac}$, (b) THD plot of inductor current with control-1.2% of the load currentat $2f_{ac}$

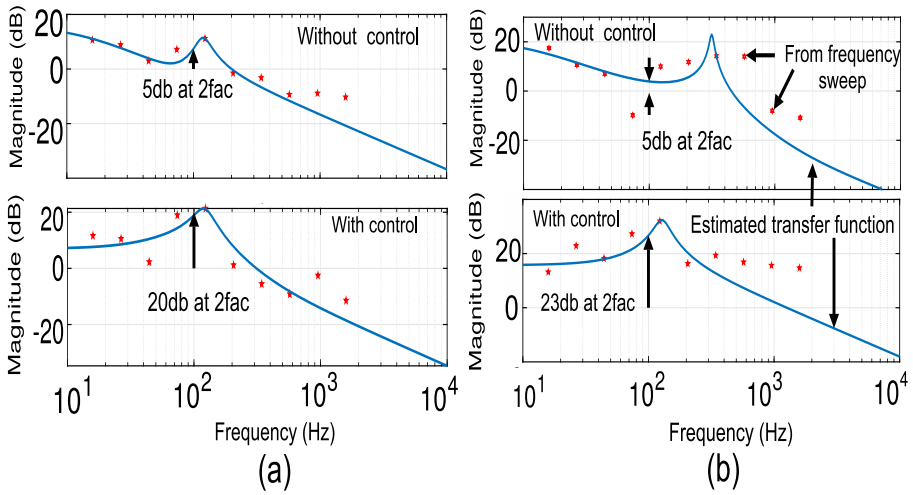

Figure 4.9 : Frequency sweep response for output impedance Zo for qZSI

To mitigate the SRC, the proposed ISMRM control is activated. The corresponding waveforms is shown in Figure 4.16. The SRC reduces to 0.3A while the capacitor voltages and ac currents remain unaffected. This verifies the effect of proposed methodology for SRC reduction in eqSBIs.

With AC load variation

The ac load is varied by 50% during T_2 and T_5 of Figure 4.18. Initially the SRC control is not activated. The SRC of 1A and 0.25A propagates to the source during T_1 and T_2. The control is implemented at interval T_4. The SRC is reduce to 0.15A from 1A. When the load is varied by 50%, the SRC is 0.1A, which was 0.25A without control.

The dc capacitor voltage remains within 10% of the desired 90V. It is observed that the voltage drop reduces compared to only dual loop control. Hence, the proposed ISMRM control is effective in reducing SRCs even during load variations while regulating the voltage transients.

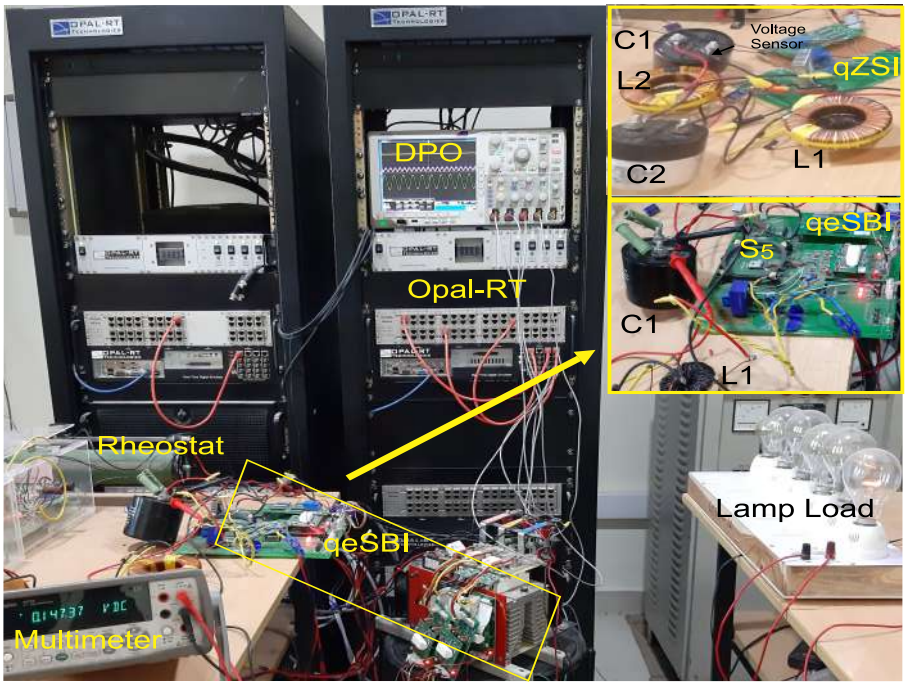

Figure 4.10 : Hardware setup for qZSI and eqSBI

SRC reduction with disturbances

The proposed control must reduce SRC in uncertain conditions. To verify this feature, the voltage reference is added with a sinusoidal disturbance of 50Hz and amplitude 5V. The voltage and current waveforms with disturbance is shown during T_1 of Figure 4.19. The zoomed section shows that the current consists of a 50Hz and 100Hz component. The proposed control is activated during T_2. It can be observed that the SRC is mitigated and current peaks due to SRC gets reduced. The disturbance is removed during the interval T_3. The SRC is reduced from 0.4A to 0.1A. Hence, the proposed control effectively reduces SRC under uncertain conditions. The effect of cancellation of disturbance can be seen from Fig. 4.20. Once the control is implemented, the uncertain oscillations due to erroneous voltage reference has been mitigated.The output AC voltage is maintained within the regulation limits and is not affected due to uncertainty mitigation.

4.7 CONCLUSION

This chapter has proposed ISMRM control technique which is applicable for SSIs. The proposed methodology has been verified to reduce SRC in qZSI and eqSBI during load transients and bounded known uncertainties. The proposed methodology increases the impedance virtually in series with the inductor near the source terminals. In qZSI, the SRC is reduced from 1A to 0.2A for a 4A load which is about 25% to 5% reduction. Similarly, in eqSBI, the SRC is mitigated from 1A to 0.15A for a 2A load which is about 50% to 7.5% reduction. The SRC reduction is maintained when the load is varied by about 50%. The dynamics of the SSI in dual loop control is improved by addition of proposed control during uncertainty. The proposed ISMRM control has been verified through simulations and experimentation for two topologies and can be applied to several other SSI topologies such as Switched Inductor ZSI ,Trans-ZSI, Inverse Watkins–Johnson topology, DC-link type SBIs etc which have either a single inductor , capacitor or a pair of inductors and capacitors.

Uptill now, the robust SRCs control methodologies for single stage inverters have been proposed. The SRCs are reflected in the DC Microgrid, when an inverter fed load is connected to the dc bus. As a result, a distributed SRC control method is required which can be integrated with the secondary control to achieve proportional load sharing and acceptable voltage regulation limits. The next chapter consists of SRC regulation in a distributed environment like the DC Microgrid. The individual nodes consists of a dual

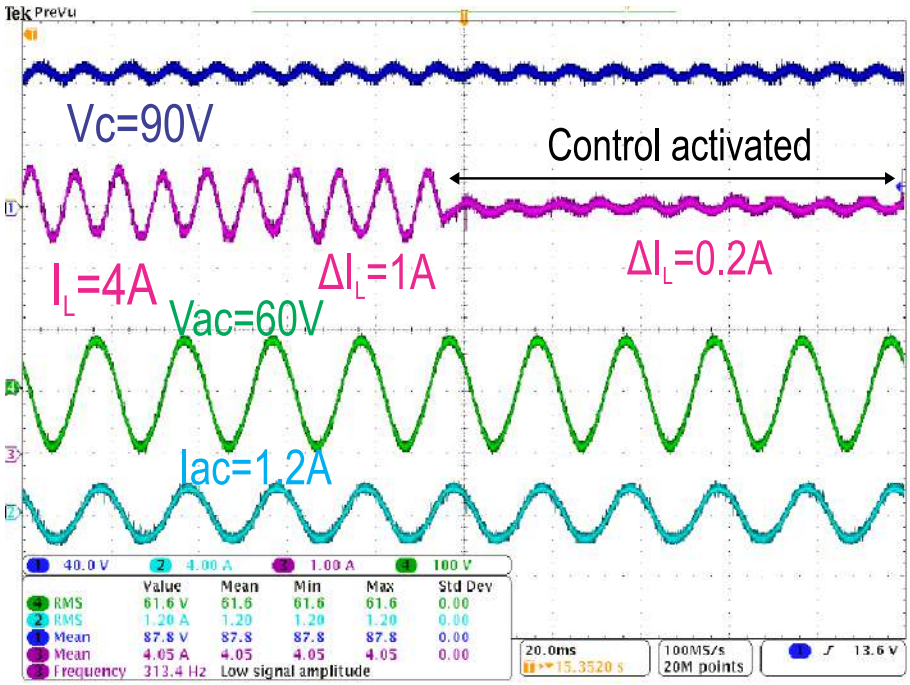

Figure 4.11 : Waveforms of qZSI with control activation

loop controller. A separate loop is designed to increase or decrease the virtual impedance, depending on the SRC reference given to the node. The proposed control is used to divert the SRCs at a node instead of being propagated at all the nodes of the DC Microgrid.

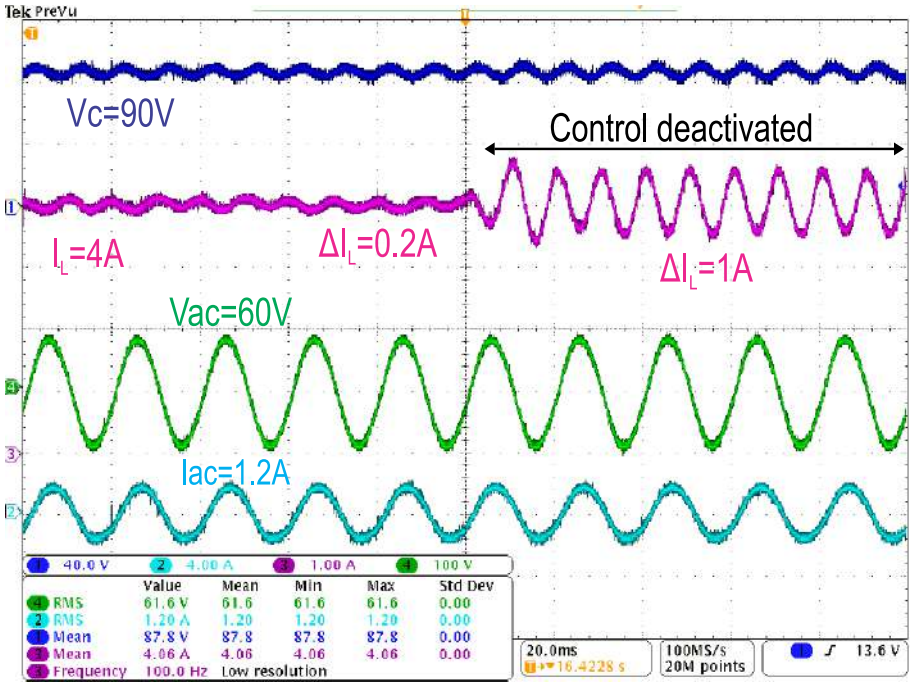

Figure 4.12 : Waveforms of qZSI with control deactivation

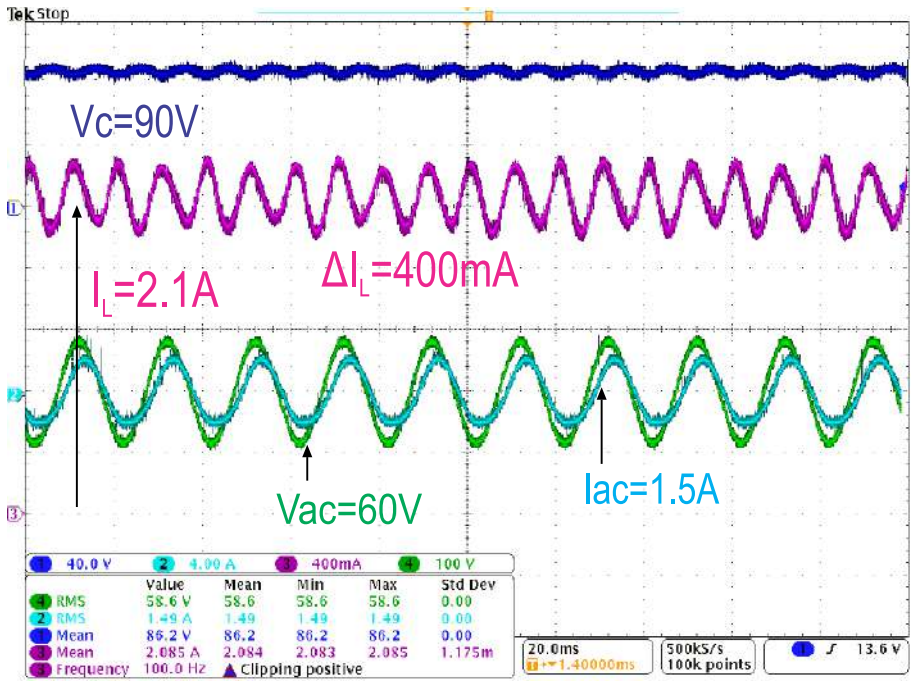

Figure 4.13 : qZSI with inductive load and control deactivated

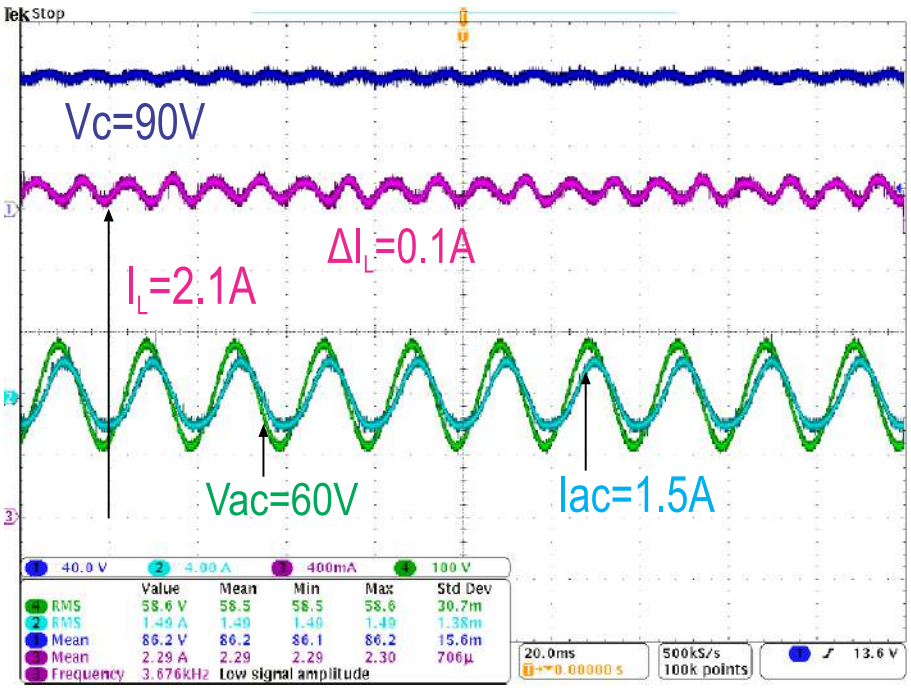

Figure 4.14 : qZSI with inductive load and control activated

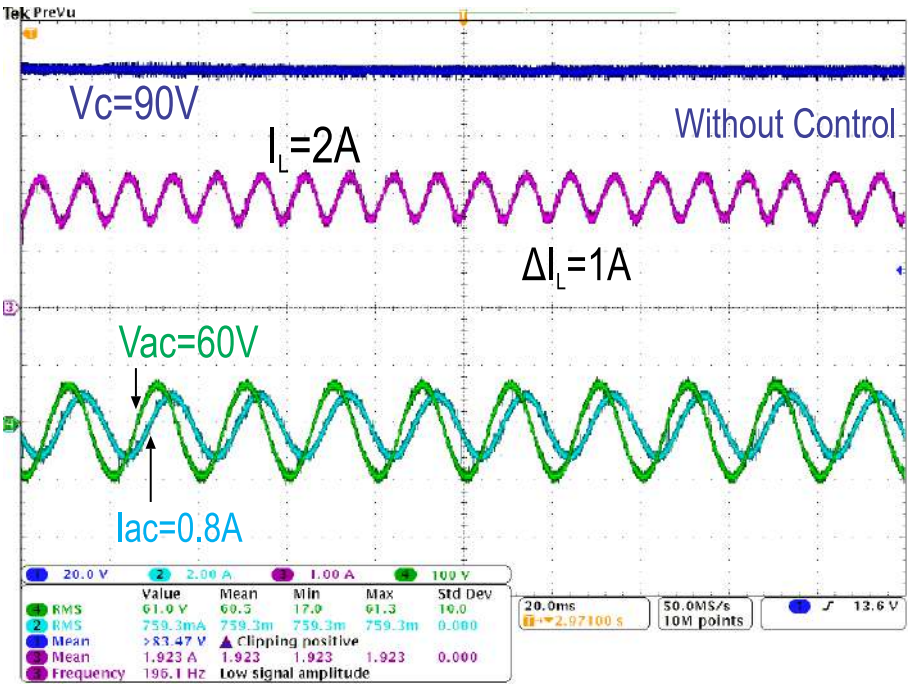

Figure 4.15 : eqSBI waveforms without control

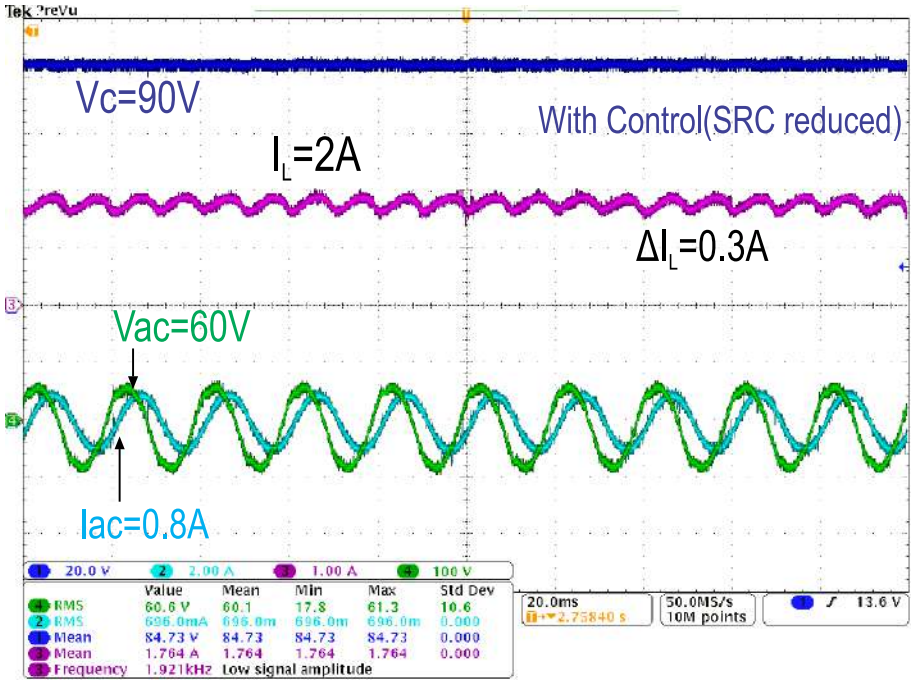

Figure 4.16 : eqSBI waveforms without control

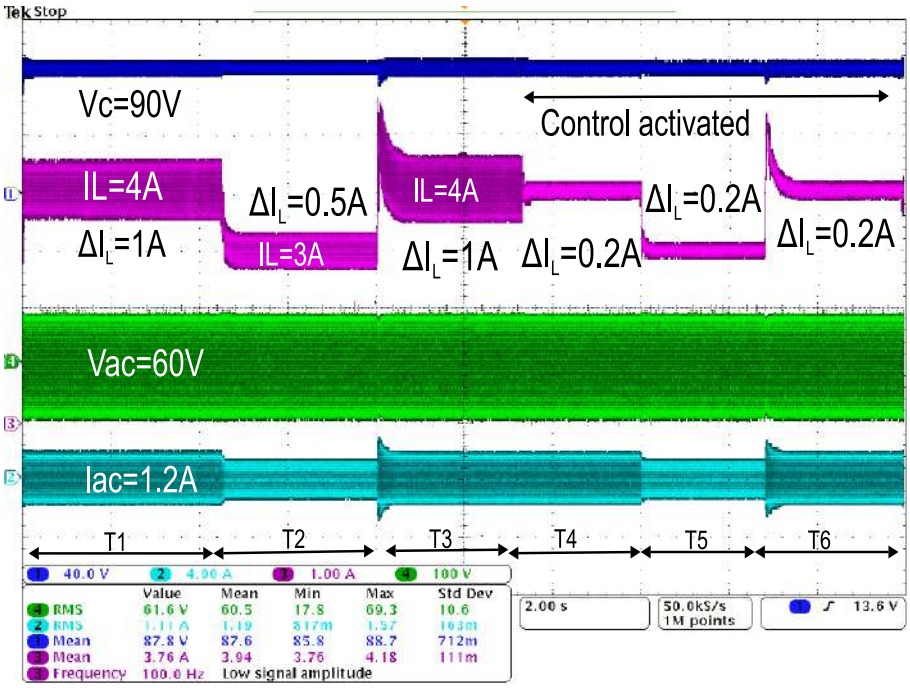

Figure 4.17 : SRC reduction with load variation for qZSI

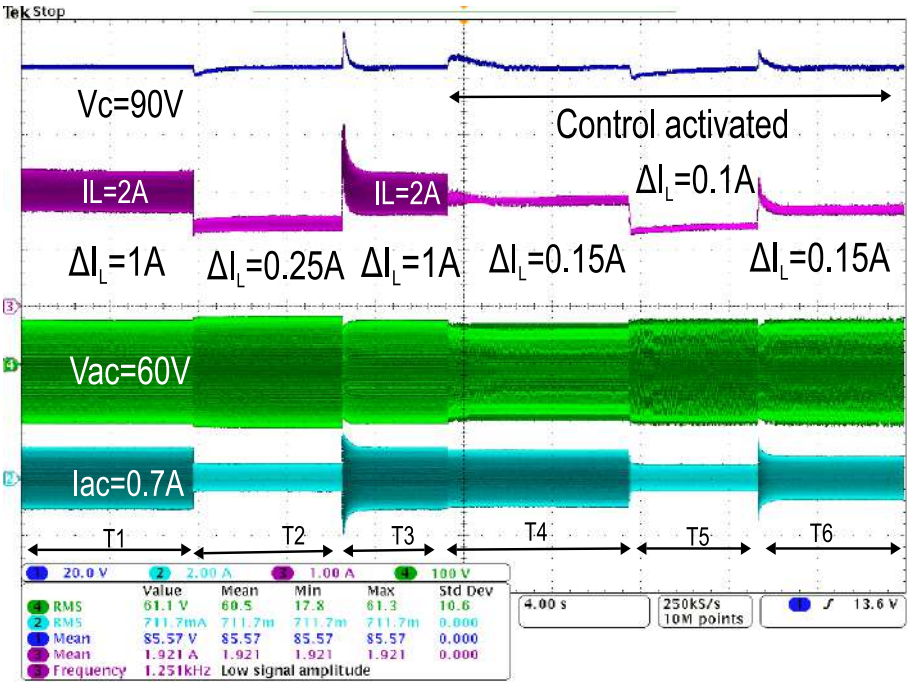

Figure 4.18 : Waveforms of eqSBI with load variations

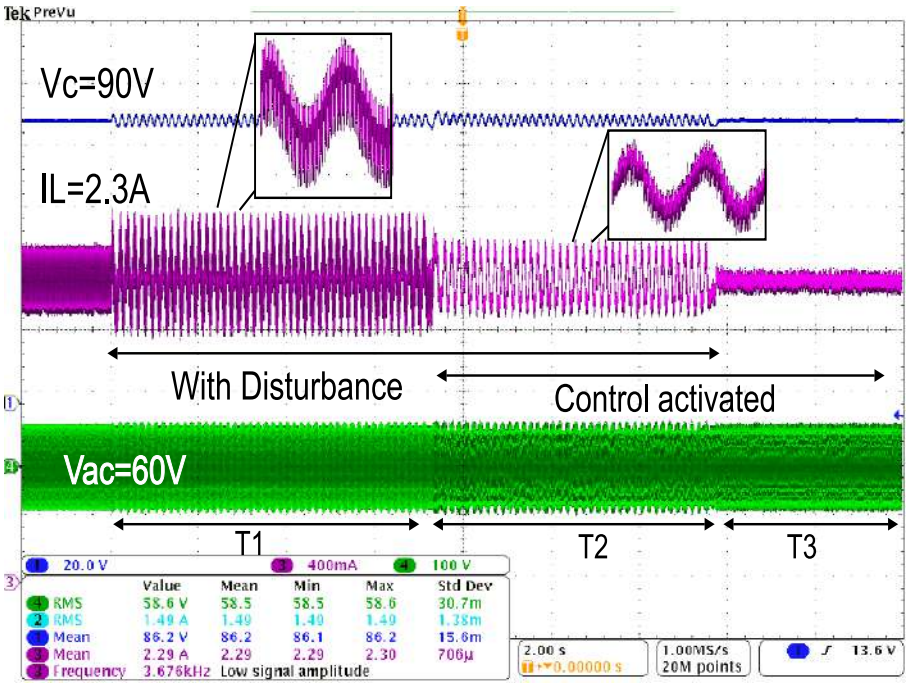

Figure 4.19 : Waveforms with sinusoidal disturbance

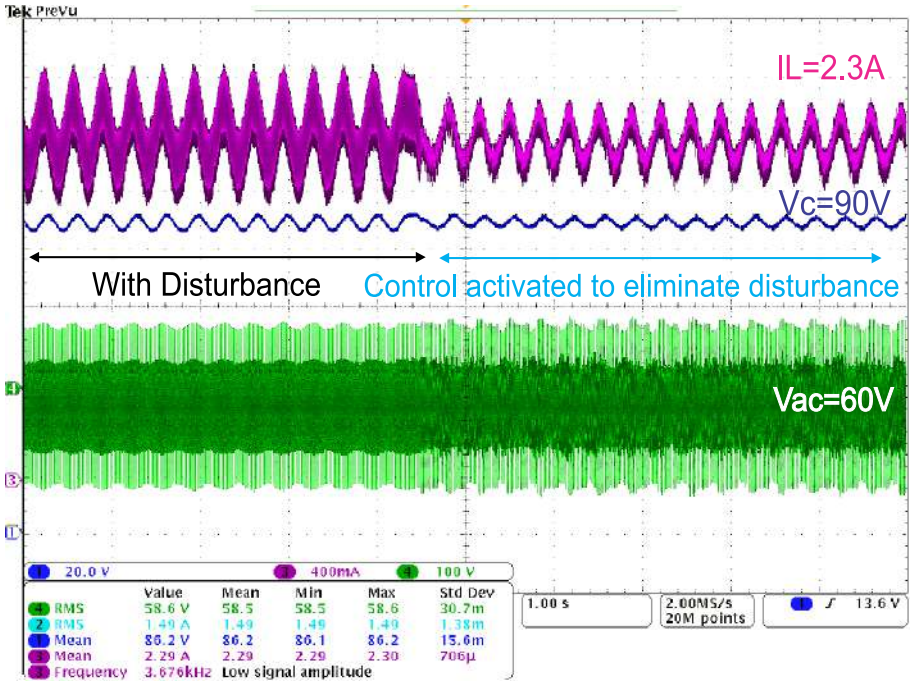

Figure 4.20 : Cancellation of disturbance using the proposed control